Published in final edited form as:
Proc IEEE Ultrason Symp. 2008 ; : 570–573. doi:10.1109/ULTSYM.2008.0137.

Development of a Multi-modal Tissue Diagnostic System Combining High Frequency Ultrasound and Photoacoustic Imaging with Lifetime Fluorescence Spectroscopy

Yang Sun,
Biomedical Engineering, University of California, Davis, Davis, CA

Douglas N. Stephens,
Biomedical Engineering, University of California, Davis, Davis, CA

Jesung Park,
Biomedical Engineering, University of California, Davis, Davis, CA

Yinghua Sun,
Biomedical Engineering, University of California, Davis, Davis, CA

Laura Marcu,
Biomedical Engineering, University of California, Davis, Davis, CA

Jonathan M. Cannata, and
Biomedical Engineering, University of Southern California, Los Angeles, CA

K. Kirk Shung
Biomedical Engineering, University of Southern California, Los Angeles, CA

Yang Sun: ywsun@ucdavis.edu; Laura Marcu: lmarcu@ucdavis.edu

Abstract

We report the development and validate a multi-modal tissue diagnostic technology, which combines three complementary techniques into one system including ultrasound backscatter microscopy (UBM), photoacoustic imaging (PAI), and time-resolved laser-induced fluorescence spectroscopy (TR-LIFS). UBM enables the reconstruction of the tissue microanatomy. PAI maps the optical absorption heterogeneity of the tissue associated with structure information and has the potential to provide functional imaging of the tissue. Examination of the UBM and PAI images allows for localization of regions of interest for TR-LIFS evaluation of the tissue composition. The hybrid probe consists of a single element ring transducer with concentric fiber optics for multi-modal data acquisition. Validation and characterization of the multi-modal system and ultrasonic, photoacoustic, and spectroscopic data coregistration were conducted in a physical phantom with properties of ultrasound scattering, optical absorption, and fluorescence. The UBM system with the 41 MHz ring transducer can reach the axial and lateral resolution of 30 and 65 μm, respectively. The PAI system with 532 nm excitation light from a Nd:YAG laser shows great contrast for the distribution of optical absorbers. The TR-LIFS system records the fluorescence decay with the time resolution of ~300 ps and a high sensitivity of nM concentration range. Biological phantom constructed with different types of tissues (tendon and fat) was used to demonstrate the complementary information provided by the three modalities. Fluorescence spectra and lifetimes were compared to differentiate chemical composition of tissues at the regions of interest determined by the coregistered high resolution UBM and PAI image. Current results demonstrate that the fusion of these techniques enables sequentially detection of functional, morphological, and compositional features of biological tissue, suggesting potential applications in diagnosis of tumors and atherosclerotic plaques.

Keywords

ultrasound backscatter microscopy; photoacoustic imaging; time-resolved fluorescence spectroscopy; multi-modal system; data coregistration

I. Introduction

Optical fluorescence spectroscopy can detect chemical compositions of tissues that allows for differentiation of normal and disease tissues [1-3]. However, due to low light penetration depth (e.g. on the order of hundreds of microns for UV excitation) the optical technique is limited by the ability to interrogate the tissue in its cross-section, which can be enhanced by the combination with imaging techniques (e.g. ultrasound or photoacoustic imaging) providing structural definition of the investigated tissue within several millimeters in depth.

High frequency ultrasound imaging can provide high resolution images of the cross-section of tissue and can also be used for tissue characterization with various algorithms (e.g. quantification of the integrated backscatter, assessment of the radiofrequency envelope, and spectral analysis of the radiofrequency signal), which has broad applications to study the microstructure of various biological systems [4-5].

Photoacoustic imaging has the advantages of both the contrast of optical imaging techniques and the depth of penetration and resolution of ultrasound imaging, providing functional image of tissues by mapping the internal tissue structure depicting the spatial distribution of optical absorbers [6]. Recent reports demonstrated that photoacoustic microscopy can retrieve functional information such as morphological relationship between a melanoma tumor and the surrounding blood vessels, angiogenesis and blood hemoglobin associated with oxygen saturation [7]. Photoacoustic imaging was also reported as a potential technique to characterize atherosclerotic plaques [8].

The overall objective of this project is to develop a multi-modal high-resolution technology for tissue characterization. Three complementary techniques are combined into one unique system including (a) ultrasound backscatter microscopy (UBM) which provides a visual reconstruction of tissue microanatomy, (b) photoacoustic imaging (PAI) which allows for mapping of optical absorption associated to specific morphology and physiology of tissue, and (c) time-resolved laser-induced fluorescence spectroscopy (TR-LIFS) which provides a direct evaluation of tissues composition.

II. Methods

A. Design of the Hybrid Probe

A hybrid probe (Ultrasonic Transducer Resource Center, University of Southern California) was constructed for acquiring multi-modal data by combing a high frequency single element ring transducer and a concentric optical fiber. The transducer was used for collection of both UBM images with pulse-echo mode and collection of the photoacoustic signals generated by the excitation of a short laser pulse using one-way mode. The optical fiber also played a dual role, delivering the pulsed 337 nm excitation light for TR-LIFS and collecting the fluorescence emission (360-660 nm) from tissue, and delivering the laser light of 532 nm for photoacoustic signal generation.

The experimental setup and transducer performance were shown in Fig. 1. The combined probe was controlled by a linear stage for scanning and immersed in a water bath for ultrasound coupling (Fig. 1a). The transducer was made with the material of lithium niobate,

with a center frequency of 41 MHz, the aperture size of 3.75 mm and the 1 mm diameter of center hole, focal length of 6 mm, and bandwidth of 63% (Fig. 1b). The 600 μm optical fiber was inserted in the center hole of the transducer with a numerical aperture of 0.22. Using this compact design of the probe, photoacoustic, ultrasonic, and spectroscopic data were easily collected sequentially.

B. UBM/TR-LIFS Combined Subsystem

A combined UBM and TR-LIFS system (Fig. 2) was developed in our research group [9-10]. For the TR-LIFS subsystem, the excitation light (337 nm) was from a N_2 laser with a pulse width of 0.8 ns and delivered to the single optical fiber through a beam splitter. Fluorescence light was collected by the same fiber, dispersed by a monochromator (MicroHR, Horiba Jobin Yvon), detected by a gated MCP-PMT (R5916U-50, Hamamatsu), amplified and digitized by an oscilloscope (DPO 7254, 2.5 GHz bandwidth, 20 Gsamples/s, Tektronix). In the UBM subsystem, a pulser up to 100 MHz and 200Vpp (AVB2-TE-C, Avtech Electrosystems) was used to drive the transducer. Echoes was amplified by a low noise amplifier with 30 dB gain and digitized by the 12-bit 400-Msamples/s acquisition board (CompuScope 12400, Gage Applied Technologies). Linear servo motor with 1 μm resolution was used to scan and control the transducer. The TR-LIFS and UBM components were fully combined and automated by one computer.

C. PAI Subsystem

The PAI system used a Nd:YAG laser source (532 nm, 8 ns pulse, 10 Hz repetition rate) and shared the receiving circuit with the UBM system (Fig. 3). The light was delivered through the optical fiber and PA signals were detected by the transducer. Maximum energy of the excitation laser light from the optical fiber was up to 400 μJ resulting in the fluence up to 10 mJ/cm^2.

According to the control procedure of the multi-modal system, after the PAI was first performed, N_2 laser source was manually switched for TR-LIFS measurements. The UBM image was acquired and the region of interest for TR-LIFS was determined from both the PAI and UBM images.

D. Design of the Multi-modal Phantom

To validate the performance of the UBM-PAI-TRLIFS system, physical and biological tissue phantoms were developed which incorporated optical and ultrasound contrast and fluorescence [11] (Fig. 4). The phantoms allowed for quantification of system performance including spatial resolution, penetration depth, imaging contrast, sensitivity, acquisition speed, and data co-registration. To create areas of optical absorption and fluorescence, 0.1% fine graphite particles and fluorophores (collagen or elastin) were mixed and embedded at the same depth in an agar matrix. Silicon dioxide particles were used in the agar matrix to be the ultrasound scatterers. Beef tendon (collagen) with pencil leads (optical absorption) was used as the biological phantom. A phantom with different types of tissues, tendon (collagen) and fat (lipid), was additionally used to see if collagen and lipid can be differentiated by photoacoustic system at the specific wavelength of 532 nm for the application of atherosclerosis.

III. Results

A. Characterization of the TR-LIFS, UBM, and PAI system

The TR-LIFS system can record fluorescence signals with a temporal resolution of ~300 ps, and a high sensitivity which can detect nM concentration. Data acquisition speed was 0.6 s/λ (could be micro-seconds using simultaneous time- and wavelength-resolved spectroscopy

[12]). The imaging system performance was estimated by imaging a sub-resolution wire target (13 μm). UBM can reach axial and lateral resolution of 37 μm and 65 μm, while photoacoustic system had the axial and lateral resolution of 50 μm and 70 μm, respectively.

B. System Validation Using the Multi-modal Physical Phantom

Multi-modal measurements and data coregistration from the physical phantom were demonstrated in Fig. 5. The PA image gave the distribution of the graphite particles with great contrast. The UBM image showed the structure of the phantom. Based on the comparison of the fluorescence characteristics, average collagen and elastin can be differentiated from both the emission spectrum and lifetime.

C. System Validation with the Biological Phantom

Fig. 6 summarized the multi-modal data acquired from the biological phantom, further demonstrating the complementary information from three modalities. From the PA images, the pencil leads with a greater absorption coefficient were highlighted. Weaker PA signal from tendon was observed using different displaying threshold. UBM image showed the cross-section of the phantom with two pencil leads embedded in the tendon tissue. From the composite UBM-PAI image, the region of interest was easily located for TR-LIFS measurements. Since the tendon layer above the pencil lead was ~ 400 μm, which UV light can not penetrate, the fluorescence signal showed the features of collagen, the major components in the tendon. Therefore, the limitation of penetration depth in the TR-LIFS technique was enhanced by the two imaging methods.

D. Multi-modal Data from Different Type of Tissues

In arterial vessels, the contrast in PAI is related to the optical absorption contrast exhibited by intima, media, adventitia, and plaques. Phantom with different tissues including tendon and fat was used to simulate the biochemical compositions of collagen and lipid in atherosclerotic plaques. In spite of the fact that PA excitation wavelength was not tunable in this system, collagen and lipid was differentiable for the specific wavelength of 532 nm using the PAI, where tendon showed stronger PA signals than the fat tissue. In the emission spectra with absolute intensity, collagen in the tendon showed greater fluorescence intensity than the lipid in the fat (small plots in Fig. 7d). Although overlapped spectra were shown in the normalized emission spectra (large plots in Fig. 7d) resulting in difficult differentiation from the shape of the spectra, fat and tendon were easily distinguished from the average lifetime, demonstrating the advantages of time-resolved measurements compared to common intensity measurements.

IV. Discussions

A. System Integration and Improvments

Currently the TR-LIFS and PA system was switched by changing the TR-LIFS fibers to PA fiber, a flip mirror will be built for changing the laser sources. The TRLIFS-UBM subsystem and PAI subsystem can be fully integrated and automated by developing the software that allows for sequential triggering of each modality. The newly developed simultaneous time- and wavelength-resolved spectroscopy system can be used to replace the TR-LIFS components which will greatly improve the data acquisition speed and then data acquisition with 2D scanning will be feasible.

B. Applications

The designed multi-modal system can be translated into intravascular use taking advantage of the IVUS machine and catheter for detection of atherosclerotic cardiovascular disease.

The system can also be used for the animal tumor model system, where TR-LIFS provides tissue autofluorescence due to collagen, NADH and porphyrin; UBM will delineate microstructures within the tumor volume; and PAI will map the angiogenesis within tumor volume.

V. Conclusions

We developed a multi-modal tissue diagnostic system combining UBM, PAI, and TR-LIFS components. The system was characterized and validated using both physical and biological phantoms. The results presented here demonstrated that: (a) spatially-correlated ultrasonic, photoacoustic, and TR-LIFS studies were feasible with the available probe; (b) the UBM and PAI composite image could be used as a guidance tool to indicate interested tissue areas for subsequent fluorescence studies; (c) great contrast originated from the optical absorption detected by PAI demonstrated that PAI could provide complementary functional information on tissue features. The resulting system can make sequential detection of morphological, functional, and compositional features of biological tissues and thus facilitated a more complete characterization of tissues, suggesting potential applications in diagnosis of human diseases such as atherosclerotic plaques and tumors.

Acknowledgments

We would like to thank Jennifer Phipps for developing the signal processing GUI, Matthew Lam for fabricating the phantom and signal processing.

This work was supported by NIH R01 HL 067377 and the UC Davis, Clinical Translational Science Center (CTST) funding.

References

1. Marcu L, Fang Q, Jo JA, Papaioannou T, Dorafshar A, Reil T, Qiao JH, Baker JD, Freischlag JA, Fishbein MC. In vivo detection of macrophages in a rabbit atherosclerotic model by time-resolved laser-induced fluorescence spectroscopy. Atherosclerosis. 2005; 181:295–303. [PubMed: 16039283]
2. Christov A, Dai E, Drangova M, Liu L, Abela GS, Nash P, McFadden G, Lucas A. Optical detection of triggered atherosclerotic plaque disruption by fluorescence emission analysis. Photochemistry and photobiology. 2000; 72:242–252. [PubMed: 10946579]
3. Arakawa K, Isoda K, Ito T, Nakajima K, Shibuya T, Ohsuzu F. Fluorescence analysis of biochemical constituents identifies atherosclerotic plaque with a thin fibrous cap. Arteriosclerosis, thrombosis, and vascular biology. 2002; 22:1002–1007.
4. Jang IK, Bouma BE, Kang DH, Park SJ, Park SW, Seung KB, Choi KB, Shishkov M, Schlendorf K, Pomerantsev E, Houser SL, Aretz HT, Tearney GJ. Visualization of coronary atherosclerotic plaques in patients using optical coherence tomography: comparison with intravascular ultrasound. Journal of the American College of Cardiology. 2002; 39:604–609. [PubMed: 11849858]
5. Komiyama N, Berry GJ, Kolz ML, Oshima A, Metz JA, Preuss P, Brisken AF, Pauliina MM, Yock PG, Fitzgerald PJ. Tissue characterization of atherosclerotic plaques by intravascular ultrasound radiofrequency signal analysis: an in vitro study of human coronary arteries. American heart journal. 2000; 140:565–574. [PubMed: 11011329]
6. Xu MH, Wang LV. Photoacoustic imaging in biomedicine. Review of Scientific Instruments. 2006; 77:041101 1–22.
7. Wang LV. Tutorial on photoacoustic microscopy and computed tomography. IEEE Journal of Selected Topics in Quantum Electronics. 2008; 14:171–179.
8. Sethuraman S, Aglyamov SR, Amirian JH, Smalling RW, Emelianov SY. Intravascular photoacoustic imaging using an IVUS imaging catheter. IEEE Transactions on Ultrasonics Ferroelectrics and Frequency Control. 2007; 54:978–986.

9. Fang QY, Papaioannou T, Jo JA, Vaitha R, Shastry K, Marcu L. Time-domain laser-induced fluorescence spectroscopy apparatus for clinical diagnostics. Review of Scientific Instruments. 2004; 75:151–162.

10. Sun Y, Park J, Stephens DN, Jo JA, Sun L, Cannata JM, Saroufeem R, Shung KK, Marcu L. Development of a dual-modal tissue diagnostic system combining time-resolved fluorescence spectroscopy and ultrasound backscatter microscopy. New Journal of Physics. submitted.

11. Sun Y, Liao KC, Sun YH, Park J, Marcu L. Novel tissue phantom for testing a dual-Modality tissue diagnostic system: time-resolved fluorescence spectroscopy and high frequency ultrasound. Proceedings of SPIE Photonics West. 2008; 6870:68700D1–9.

12. Sun YH, Liu R, Elson DS, Hollars C, Jo JA, Park J, Sun Y, Marc L. Simultaneous time- and wavelength-resolved fluorescence spectroscopy for near real-time tissue diagnosis. Optics Letters. 2008; 33:630–632. [PubMed: 18347733]

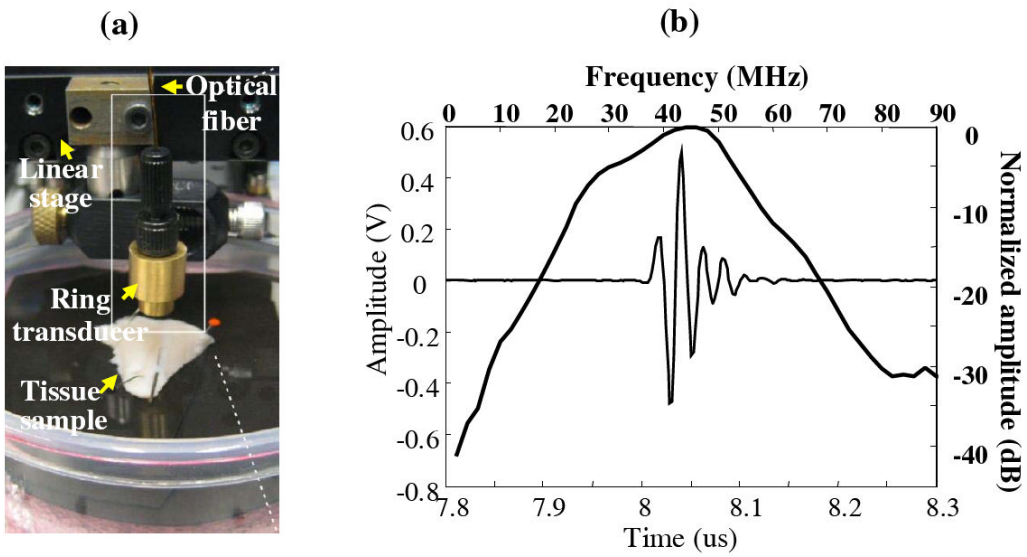

Figure 1.

(a) Picture of the experimental setup of the multi-modal UBM/PAI/TRLIFS probe integrating an ultrasound transducer and a single optical fiber with the concentric assembly. (b) Ring transducer performance showing the pulse and spectrum of the acoustic reflection from a glass surface using pulse-echo mode.

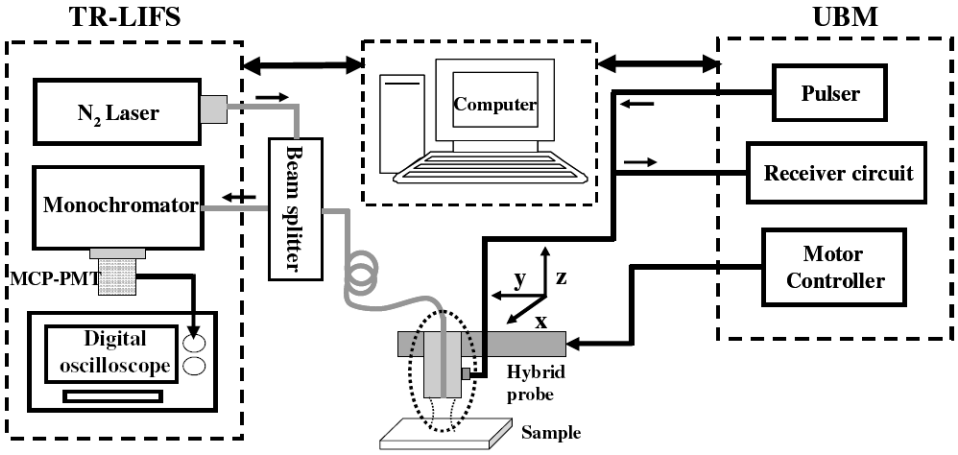

Figure 2.
Schematic diagram of the combined UBM/TR-LIFS system. The combined system consisted of the TR-LIFS subsystem, the control computer, the hybrid probe, and the UBM subsystem.

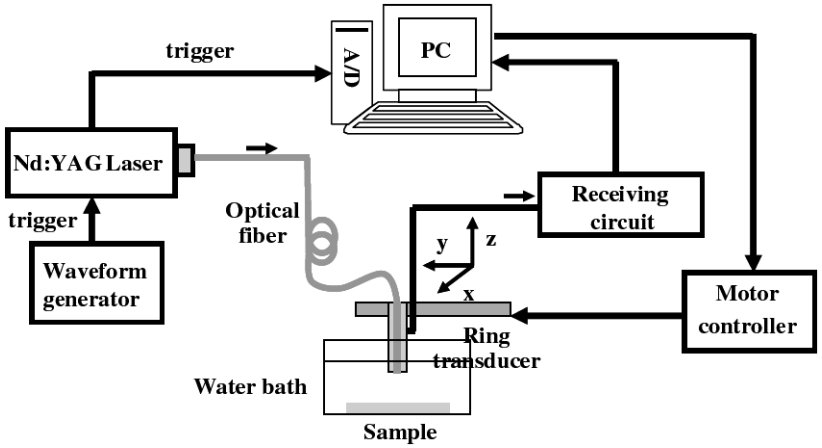

Figure 3.
The schematic diagram of the photoacoustic system.

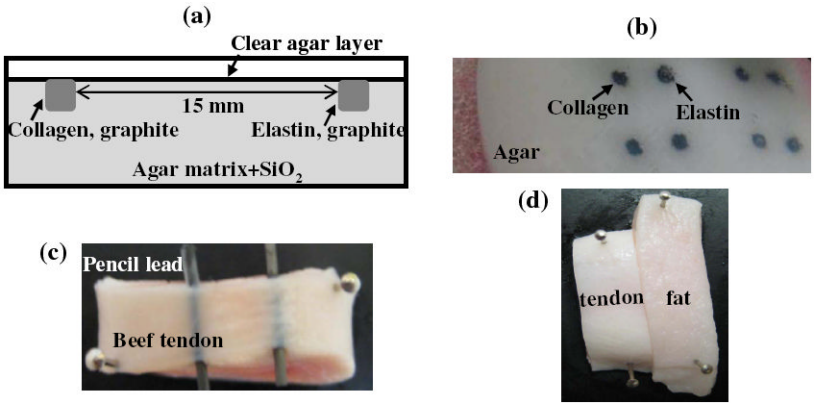

Figure 4.

(a) Illustration of the multi-modal phantom design; (b) photo of the phantom; (c) photo of the biological phanton including beef tendon and pencil leads; (d) phantom with different types of tissues (tendon and fat).

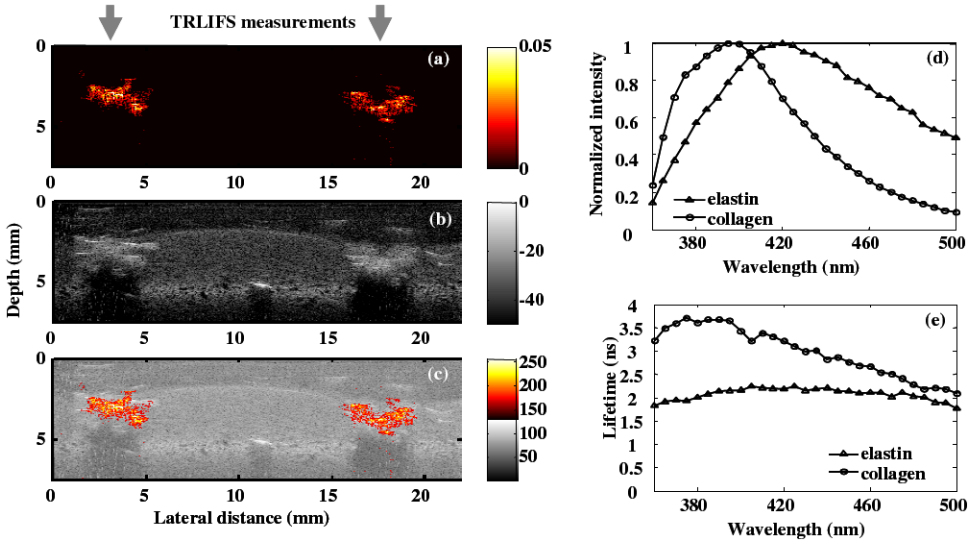

Figure 5.

(a) PA image showing the distribution of the absorbers; (b) UBM image showing the structure of the phantom; (c) composite UBM and PA image; (d) comparison of the average emission spectra and (e) average lifetime as a function of wavelength between collagen and elastin.

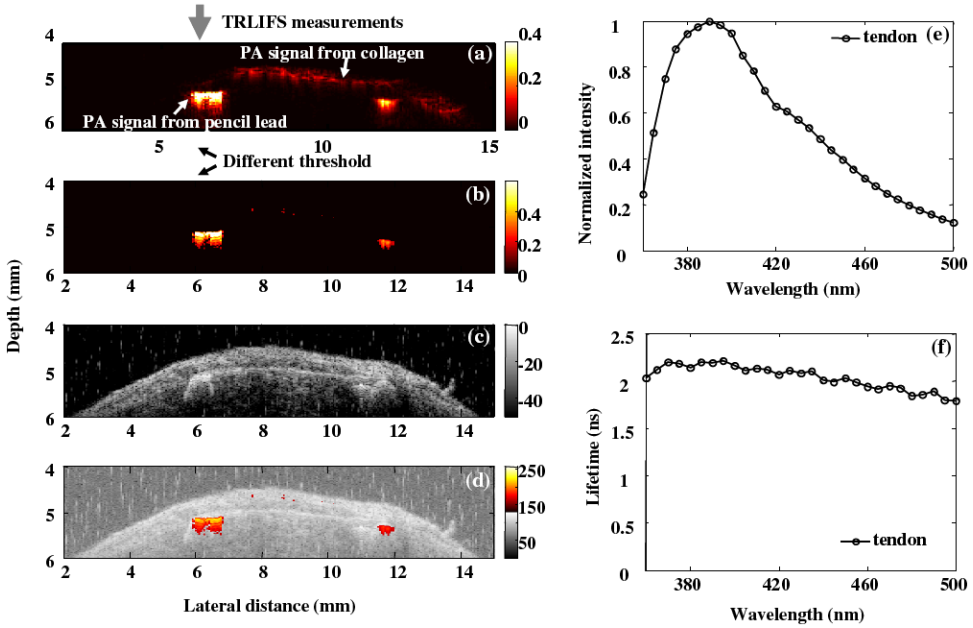

Figure 6.

(a) PA image showing signals from collagen and pencil leads (b) PA image with different displaying threshold showing only the pencil leads with greater absorbance; (c) UBM image showing the structure of the phantom; (d) composite UBM and PA image; (e) the average emission spectra and (f) average lifetime as a function of wavelength from tendon.

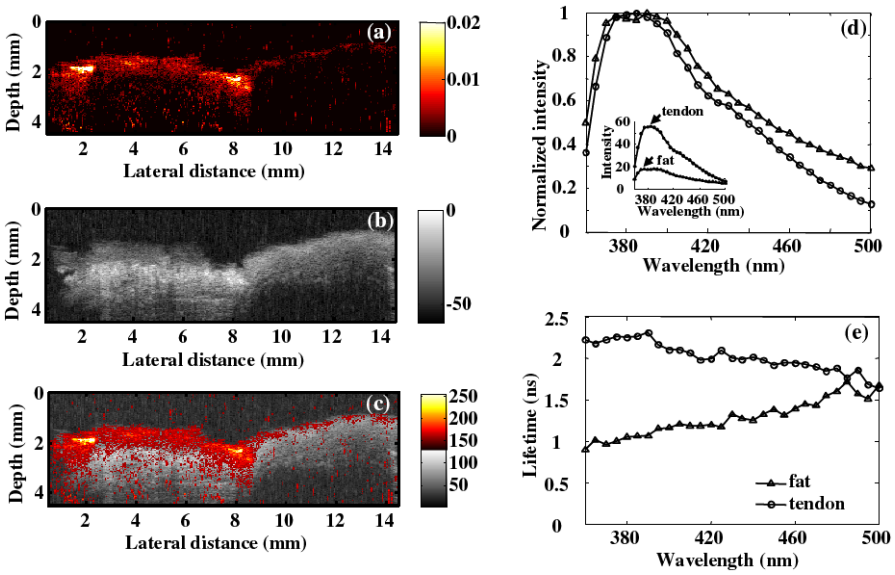

Figure 7.

(a) PA image showing different ability of optical absorbance of collagen and lipid @ 532 nm; (b) UBM image showing the structure of the phantom; (c) composite UBM and PA image; (d) comparison of the absolute (small plots) and normalized (large plots) spectra, where showed that the absolute intensity of the fat fluorescence was lower than the tendon intensity while the normalized spectra from tendon and fat overlapped; (e) comparison of average lifetime as a function of wavelength between tendon and fat showing the ability to differentiate the fat and tendon from lifetime.